NASA TECHNICAL NOTE

NASA TN D-5386

EXPERIMENTS ON THE STEADY-STATE CHARACTERISTICS OF HERRINGBONE-GROOVED AIR-LUBRICATED JOURNAL BEARINGS

by Robert E. Cunningham, David P. Fleming, and William J. Anderson

Lewis Research Center
Cleveland, Ohio

NATIONAL AERONAUTICS AND SPACE ADMINISTRATION • WASHINGTON, D. C. • AUGUST 1969

EXPERIMENTS ON THE STEADY STATE CHARACTERISTICS OF HERRINGBONE-GROOVED AIR-LUBRICATED JOURNAL BEARINGS

By Robert E. Cunningham, David P. Fleming, and William J. Anderson

Lewis Research Center
Cleveland, Ohio

NATIONAL AERONAUTICS AND SPACE ADMINISTRATION

For sale by the Clearinghouse for Federal Scientific and Technical Information
Springfield, Virginia 22151 – CFSTI price $3.00

ABSTRACT

Experiments were conducted with five rotors $1\frac{1}{2}$ in. (3.81 cm) in diameter and equipped with two herringbone-grooved patterns. Results showed that a range of groove- to ridge-clearance ratios of 2.0 to 2.4 has greater load capacities than do ratios greater or less than this optimum range. Load capacity increases with eccentricity ratio at a rate greater than linear. Agreement with a small-eccentricity pressure perturbation theory was good for groove- to ridge-clearance ratios in this optimum range but only at eccentricity ratios less than 0.3. These rotors were operated under unidirectional loading to a maximum compressibility number of 45.

EXPERIMENTS ON THE STEADY-STATE CHARACTERISTICS OF HERRINGBONE-GROOVED AIR-LUBRICATED JOURNAL BEARINGS

by Robert E. Cunningham, David P. Fleming, and William J. Anderson

Lewis Research Center

SUMMARY

Experiments were conducted with five rotors, $1\frac{1}{2}$ inches (3.81 cm) in diameter by $12\frac{1}{4}$ inches (31.1 cm) long and equipped with two herringbone-grooved patterns. Results showed that a range of groove- to ridge-clearance ratios of 2.0 to 2.4 has greater load capacity than ratios greater or less than this optimum range. Load capacity increases with eccentricity ratio at a rate greater than linear. Experimental results agreed well with a small-eccentricity perturbation theory for rotors whose groove geometries fell within this optimum range but only at eccentricity ratios less than 0.3. At high eccentricity ratios and compressibility numbers, the load capacity for three of the five rotors tested exceeded the theoretical.

Negative bearing attitude angles were predicted by the theory and were also obtained experimentally. Although measured attitude angles were, in general, slightly higher than the theoretical, the agreement in most cases was quite good.

These rotors were operated in two plain cylindrical bronze sleeves. The maximum speed attained was 60 000 rpm, which corresponds to a compressibility number of 45. Steady unidirectional loads were varied up to 20.8 pounds per square inch (14.3 N/cm^2) of the projected bearing area.

INTRODUCTION

The development of turbomachines whose bearings are lubricated by the cycle gas has resulted in a renewed interest in the hydrodynamic, or self-acting bearing. The high speeds at which the compressor turbine shafts operate, above 30 000 rpm, and the long-term reliability requirements of the machine place a decided emphasis on stable operation. This requirement precludes the use of the plain cylindrical bearing that is inher-

ently unstable at light loads (ref. 1). Also, the load capacity of a plain bearing, adequate at low speeds, approaches a constant at higher speeds (ref. 2). A number of self-acting bearing designs have evolved, most of which compromise load capacity to achieve stability. A self-acting bearing receiving considerable attention in recent years is the herringbone-grooved journal bearing. Shallow grooves in the form of a herringbone pattern (fig. 1) act like a viscous pump or compressor. Ambient air is initially pumped from the bearing ends to the bearing center. At equilibrium the pumping tendency of the bearing is matched by pressure increases along the grooves toward the bearing center. The pressure profile produced is similar to that of a hydrostatic bearing. This has been treated theoretically (ref. 3) and experimentally (ref. 4). The small-eccentricity pressure perturbation theory of reference 3 shows that load capacity increases significantly above that of a plain bearing at moderate to high compressibility numbers. Experimental results of reference 5 and 6 were obtained with a single optimized groove configuration up to a compressibility number of approximately 16. The experimental results given in reference 5 are compared with a numerical solution to the Reynolds equation applicable to herringbone-groove geometry. This approximate solution also assumes a "smoothed pressure distribution" existing in the gas film. These results do show this trend of increasing load capacity with speed.

The objectives of this study were (1) to investigate experimentally load capacity, attitude angle, and stiffness of the partially grooved herringbone bearing to high compressibility numbers and (2) to compare the results with existing small-eccentricity perturbation theory (ref. 3). The following parameters and their effects on the steady-state performance were examined: helix angle, number of grooves, and ratio of groove clearance to ridge clearance. Groove width to total groove plus land width was 0.35 for one rotor and 0.5 for all others. Bearing length-to-diameter ratio was 1, and grooved length to total bearing length was 0.6 for all bearings.

Five rotors $1\frac{1}{2}$ inches (3.81 cm) in diameter by $12\frac{1}{4}$ inches (31.1 cm) long, each containing two herringbone-groove patterns, were tested to compressibility numbers of 45. The rotors were mounted horizontally in two plain cylindrical bronze sleeves. Applied loads varied up to 46.8 pounds (208 N) per bearing or 20.8 pounds per square inch (14.3 N/cm^2) of the projected bearing area. Different sets of bronze sleeves were used with the rotors to provide a range of zero-speed radial clearances from 320 to 650 microinches (8.1 to 16.5 μm).

SYMBOLS

a_g width of helical groove, in.; mm

a_r width of helical land, in.; mm

C	bearing radial clearance, μin.; μm
D	rotor diameter, in.; cm
e	rotor eccentricity, in.; mm
H	ratio of groove clearance to ridge clearance, h_g/h_r
h_g	groove clearance at zero eccentricity, in.; mm
h_r	ridge clearance at zero eccentricity, in.; mm
K	film stiffness, psi; N/m^2
$\overline{K}$	dimensionless stiffness, CK/P_aLD
L	bearing length, in.; cm
L_1	length of grooved portion of bearing, in.; cm
N	shaft speed, rpm
n	number of grooves
P_a	atmospheric pressure, psia; N/cm^2 abs
R	rotor radius, in.; cm
W	applied load per bearing, lb; N
$\overline{W}$	dimensionless load, W/P_aLD
Y	ratio of grooved length to total bearing length, L_1/L
α	ratio of groove width to total width, groove plus land, $a_g/(a_g + a_r)$
β	helix angle, deg
ϵ	journal eccentricity ratio, e/C
δ	groove depth, $h_g - h_r$, μin.; μm
Λ	bearing compressibility number, $(6\mu\omega/P_a)(R/C)^2$
μ	absolute viscosity, (lb)(sec)/$in.^2$; (N)(sec)/m^2
φ	bearing attitude angle, deg
ω	angular rotor speed, rad/sec

APPARATUS

The apparatus used in this investigation is shown schematically in figure 2. A steel rotor $1\frac{1}{2}$ inches (3.81 cm) in diameter and $12\frac{1}{4}$ inches (31.1 cm) long is supported horizontally in two bronze sleeves. Two identical herringbone-groove patterns etched

into the rotor surface are coincident with the sleeves and comprise a two-bearing assembly. Groove patterns extend slightly beyond the ends of the $1\frac{1}{2}$-inch- (3.81-cm-) long sleeves to ensure a supply of ambient air. The axial centerline distance between the two sleeves is $6\frac{5}{8}$ inches (16.8 cm). Steady unidirectional radial loads are applied to the rotors by means of an externally pressurized load shoe (fig. 2(a)). A spherical pivot assembly couples the load shoe to the shaft of a rolling diaphragm air cylinder. Two externally pressurized thrust bearings locate the shaft axially, and two externally pressurized radial bearings lift the shaft during startup.

The rotors are driven by an impulse turbine assembly, which consists of ten 1/8-inch- (3.2-mm-) diameter nozzles and six equally spaced turbine buckets machined into the rotor surface at one end. A solid-state electronic controller was used to regulate the turbine air supply and thus maintain a preset rotor speed.

INSTRUMENTATION

Two orthogonally oriented capacitance distance probes were located in the same radial plane and outboard of each bearing, as shown in figure 2. These probes provided a noncontacting method of detecting radial displacements of the rotor. The probes with their associated meters were calibrated with precision gage blocks. A digital voltmeter was used to read the voltage output from the probes. It was possible to discriminate readings to 1/2 millivolt, which corresponds to 2.5 microinches (0.06 μm). Journal loci were displayed on X, Y-curve-tracing cathode ray oscilloscopes. Graphic records of the changing loci were made with polaroid cameras.

TEST ROTOR AND SLEEVES

The test rotor shown in the photograph of figure 3 is typical of the five rotors investigated. Groove geometries listed in table I are all for the partially grooved, inward pumping design. The rotors were made of AMS-5643 precipitation-hardening stainless steel. Hardness varied from 42 to 45 on the Rockwell C scale. The bronze sleeves in which the rotors were assembled were line bored and lapped in place. Additional details regarding machining accuracies obtained for both rotors and sleeves are given in reference 4.

TABLE I. - CHARACTERISTIC DIMENSIONS OF HERRINGBONE-GROOVE PATTERNS TESTED

[Groove width to total width ratio, 0.5; groove length to total bearing length ratio, 0.6; rotor weight, 6.06 lb (2.75 kg); rotor length, $12\frac{1}{4}$ in. (31.1 cm); bearing span, 6.64 in. (16.9 cm); nominal rotor diameter, $1\frac{1}{2}$ in. (3.81 cm); bearing length-to-diameter ratio, 1.0.]

Rotor	Helix angle, β, deg	Number of grooves, n	Zero-speed radial clearance,[a] C		Groove depth,[b] δ		Ratio of groove clearance to ridge clearance,[a] H
			μin.	μm	μin.	μm	
A-1	30	20	400	10.2	580	14.7	2.4
			440	11.2			2.3
A-2	35	20	470	11.9	640	16.2	2.4
			480	12.2			2.3
A-3	35	23	630	16	540	13.7	1.9
			650	16.5			1.8
A-3	35	23	320	8.1	540	13.7	2.7
			340	8.6			2.6
A-5	40	28	410	10.4	710	18	2.7
			420	10.7			2.7
[c]A-7	40	40	520	13.2	540	13.7	2.0
			550	14			2.0

[a]First value, turbine end bearing; second value, thrust end bearing.
[b]Measurements made with surface profile tracer (readings averaged).
[c]Groove width to total width ratio, 0.33.

PROCEDURE

Before and after each test, the clearances in each bearing were measured by using the capacitance probes. Room temperature and barometric pressures were recorded. Air was then supplied to the two radial lifters and the loader. The rotor position was noted on the cathode ray oscilloscope to see that it was centered in each of the bearing bores. The rotor was then brought up to the desired test speed and the lifter air turned off. The radial loader was adjusted so that the applied upward force just balanced the weight of the rotor. The probe output voltages were recorded for this zero-load or zero-eccentricity position. Radial loads were applied to the test bearings by increasing the pressure to a diaphragm air cylinder in increments of either 1 or 2 pounds per square

inch (0.7 or 1.4 N/cm^2). A calibrated curve of load per bearing in pounds (kg) against cylinder pressure in pounds per square inch (N/cm^2) was used to determine bearing loading. At each incremental change in load, values of output voltage for each probe were recorded. These values were converted to distance readings and in an X- and Y- plane for each of the orthogonally mounted probes (fig. 2). After a maximum safe load was reached for that speed, the load was completely removed and the speed increased to some new value. At the new speed, the foregoing procedure was repeated.

RESULTS AND DISCUSSION

Experimental results obtained with five herringbone-grooved rotors are plotted in figures 4 to 10. These rotors, whose groove characteristics are listed in table I, were operated in ambient air to a maximum compressibility number of 45. Steady unidirectional loads were varied up to 20.8 pounds per square inch (14.3 N/cm^2) of the projected bearing area.

Figures 4(a) to (g) are plots of dimensionless load against eccentricity ratio for all five rotors tested. These experimental curves have the shape characteristic of most self-acting bearings in that the load capacity increases sharply for increasing eccentricity ratios. The straight dashed lines are the theoretical predictions from reference 3. Agreement between experiment and theory for rotor A-1 is only fair. The best agreement is at eccentricity ratios below 0.3 (lightly loaded rotor) and compressibility numbers less than 20. The experimental load capacity as a function of eccentricity ratio for rotors A-2, A-3, A-5, and A-7, however, is generally less than the predicted values.

In figure 4(g), a comparison is made between the data obtained for rotor A-7 and the herringbone-grooved rotor tested in reference 5. Groove geometry for the reference rotor was chosen to give maximum radial stiffness, based on theory, at a compressibility number of 20. Table II lists the parameters that differed between the two rotors.

It is interesting to note that, although the groove patterns are different, the load capacity curves correspond closely.

In figures 5(a) to (f), experimental and theoretical load capacity curves are presented at varying compressibility numbers. These experimental curves (dashed lines) are cross plots of the data in figures 4(a) to (g). The theory is based on the small-eccentricity pressure perturbation of reference 3. Agreement between theory and experiment for the groove geometry of rotor A-1 (fig. 5(a)) is only fair. Experimental values of load capacity are less than theory at low compressibility numbers but greater than theory at the higher compressibility numbers. For high-speed turbomachines, the region of greater interest is the one at high compressibility numbers. The experimental results plotted in figure 5(b) for rotor A-2 are considered good over this limited range of compressibility numbers.

TABLE II. - COMPARISON OF GROOVE

PARAMETERS FOR TWO ROTORS

	Rotor	
	A-7	Reference 5
Helix angle, β, deg	40	25
Number of grooves, n	40	36
Ratio of groove clearance to ridge clearance, H	2.00	2.33
Ratio of groove length to total length, Y	0.6	0.5
Radial clearance C, μin.; μm	520; 13.2	495; 12.6

The greatest disparity between measured and theoretical load capacity can be seen in the results plotted for rotor A-3 (figs. 5(c) and (d)), where the theory predicts considerably greater load capacity than observed experimentally. Experimental load capacity for rotors A-5 and A-7, as plotted in figures 5(e) and (f), respectively, is also less than what theory predicts. It can be concluded from these plots that the theory is optimistic in most cases for low compressibility numbers and low eccentricity ratios.

Figure 6 is a composite of the experimental curves in figures 5(a) to (f) for an eccentricity ratio of 0.3. The curves for rotors A-1, A-2, A-7, and A-3 (high clearance) are quite close together, whereas the curves for rotors A-3 (low clearance) and A-5 showed considerably less load capacity. The average H value for A-1, A-2, A-7, and A-3 (high clearance) was 2.1, whereas it was 2.7 for A-5 and A-3 (low clearance). These values suggest that clearance and particularly groove-clearance to ridge-clearance ratio H have a significant effect on load capacity. The theory (ref. 3) does show that for values of H above 2.5 radial stiffness drops off sharply.

The data for all rotors show collectively that the best load capacity is obtained when H is in the range from 2.0 to 2.4. In a comparison of experimental and theoretical load capacities, experiments indicate that load capacity increases at a rate greater than linear with increasing eccentricity ratio. This contrasts with the linear prediction of theory. The load capacity of rotors with groove- to ridge-clearance ratios in the optimum range agreed well with theory at low eccentricity ratios. At high eccentricity ratios and especially at high compressibility numbers, the load capacity of the best rotors exceeded theoretical.

The dimensionless stiffness as a function of eccentricity ratio at different compressibility numbers is plotted in figure 7 for the turbine end bearing of rotor A-1. The horizontal straight lines are the theoretical stiffness curves. This constant stiffness is characteristic of a small-eccentricity pressure perturbation solution. A minimum value

of stiffness occurs at an eccentricity ratio of approximately 0.17 for compressibility numbers of 19.5 and 26.8. For lower compressibility numbers, the stiffness increases continuously with eccentricity ratio; the curves are similar in slope to experimental stiffness curves of a rotating externally pressurized air bearing (ref. 7).

The data plotted in figures 8(a) to (e) are those of the attitude-eccentricity locus in polar coordinates. In figures 8(a) to (c), a comparison is made between the experimental attitude-eccentricity locus of the herringbone-grooved bearing and that of a plain journal bearing. There is a marked similarity here between the two bearing types, particularly at the lower compressibility numbers. The most significant feature in these plots is the negative attitude angles observed at the higher compressibility numbers in figures 8(a) and (b). The attitude-eccentricity loci, as plotted in figure 8(e), are for one of the bearings of rotor A-7. Data were plotted for speeds of 10 000, 20 000, 30 000, and 40 000 rpm. The loci appearing in the photographs of figures 9(a) to (d) are for the same rotor at the same speeds and approximately the same load range. The photographs show, as do the plotted data of figures 8(a) to (e), that attitude angles decrease as rotor speed increases. The curvature of the locus also diminishes as the speed increases.

Figures 10(a) to (d) show attitude angles plotted against compressibility number. The solid curve is the small-eccentricity pressure perturbation theory (ref. 3). The theoretical attitude angles for rotor A-1 (fig. 10(a)) are negative for a compressibility number greater than about 20. The experimental data also show this behavior for compressibility numbers greater than 18. Somewhat larger negative attitude angles were observed at the highest compressibility numbers than was predicted by the theory. For most cases, measured attitude angles are somewhat greater than predicted by the theory. The best agreement is shown for rotors A-1 and A-7 (figs. 10(a) to (d)). Rotor A-3 shows the poorest agreement with theory, which was also the case for the measured dimensionless load data for this rotor (fig. 5(c)).

SUMMARY OF RESULTS

The following results were obtained with five rotors, $1\frac{1}{2}$ inches (3.81 cm) in diameter by $12\frac{1}{4}$ inches (31.1 cm) long, operating in ambient air to a maximum compressibility number of 45, corresponding to a rotor speed of 60 000 rpm. The rotors, each containing two herringbone-groove patterns at two axial locations, were operated horizontally in two cylindrical bronze sleeves. Steady unidirectional loads were varied up to 20.8 pounds per square inch (14.3 N/cm^2) of the projected bearing area.

1. An average groove- to ridge-clearance ratio H in the range of 2.0 to 2.4 showed greater load capacity than ratios greater or less than this optimum range.

2. Load capacity increased at a rate greater than linear with increasing eccentricity ratio. The load capacity of rotors with groove- to ridge-clearance ratios in the optimum range agreed well with theory at low eccentricity ratios. At high eccentricity ratios and especially at high compressibility numbers, the load capacities of rotors A-1, A-2, and A-7 exceeded the theoretical.

3. Negative attitude angles were observed with rotor A-1 at high compressibility numbers.

4. Dimensionless film stiffness curves plotted for rotor A-1 showed a minimum value at an eccentricity ratio of 0.17 at compressibility numbers of 19.5 and above.

5. Agreement between experimental and theoretical attitude angles plotted against compressibility number was quite good.

6. A comparison of experimental attitude-eccentricity loci of the herringbone-groove bearing with the theoretical plain journal bearing showed a marked similarity.

Lewis Research Center,
National Aeronautics and Space Administration,
Cleveland, Ohio, May 16, 1969,
129-03-13-05-22.

REFERENCES

1. Sternlicht, B.; and Winn, L. W.: On the Load Capacity and Stability of Rotors in Self-Acting Gas Lubricated Plain Cylindrical Journal Bearings. J. Basic Eng., vol. 85, no. 4, Dec. 1963, pp. 503-512.

2. Raimondi, A. A.: A Numerical Solution for the Gas Lubricated Full Journal Bearing of Finite Length. ASLE Trans., vol. 4, no. 1, Apr. 1961, pp. 131-155.

3. Vohr, J. H.; and Chow, C. Y.: Characteristics of Herringbone-Grooved, Gas-Lubricated Journal Bearings. J. Basic Eng., vol. 87, No. 3, Sept. 1965, pp. 568-578.

4. Cunningham, Robert E.; Fleming, David P.; and Anderson, William J.: Experimental Stability Studies of the Herringbone-Grooved Gas Lubricated Journal Bearing. J. Lub. Tech., vol. 91, no. 1, Jan. 1969, pp. 52-59.

5. Castelli, V.; and Vohr, J. H.: Performance Characteristics of Herringbone-Grooved Journal Bearings Operated at High Eccentricity Ratios and With Misalignment. Rep. MTI-67TR15, Mechanical Technology, Inc. (NASA CR-88085), Mar. 1967.

6. Malanoski, S. B.: Experiments on an Ultrastable Gas Journal Bearing. J. Lub. Tech., vol. 89, no. 4, Oct. 1967, pp. 433-438.

7. Cunningham, Robert E.; Fleming, David P.; and Anderson, William J.: Experiments on Rotating Externally Pressurized, Air Journal Bearings. I - Load Capacity and Stiffness. NASA TN D-5191, 1969.

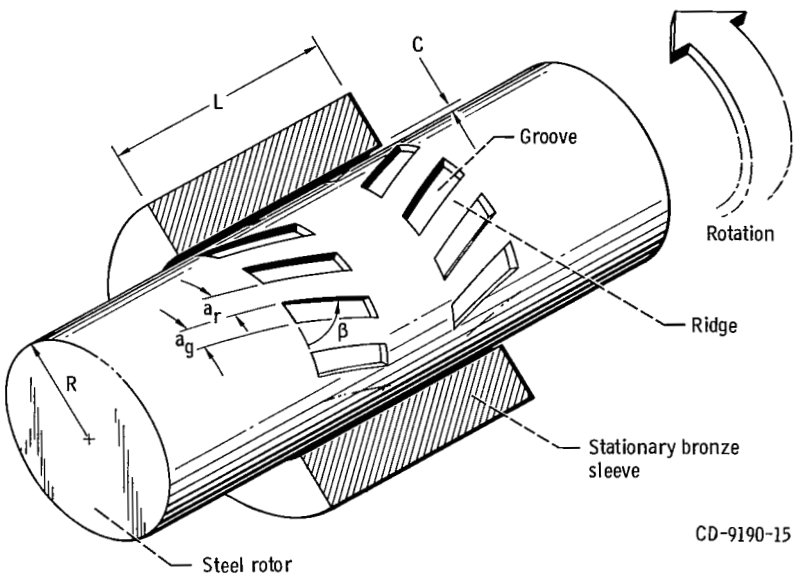

Figure 1. - Herringbone-groove pattern.

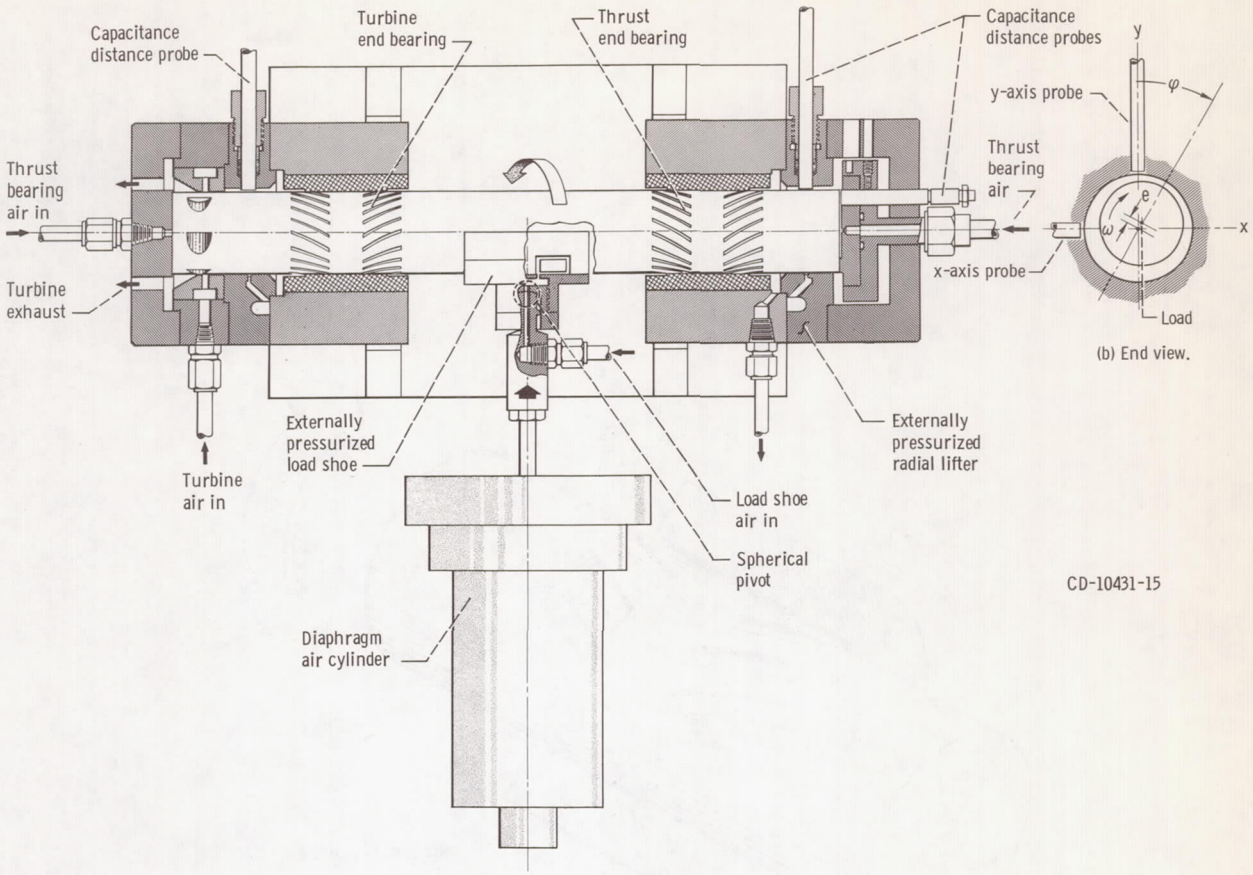

(a) Section view of rotor-bearing assembly.

Figure 2. - Test apparatus.

C-67-3608

Figure 3. - Typical herringbone-grooved test rotor.

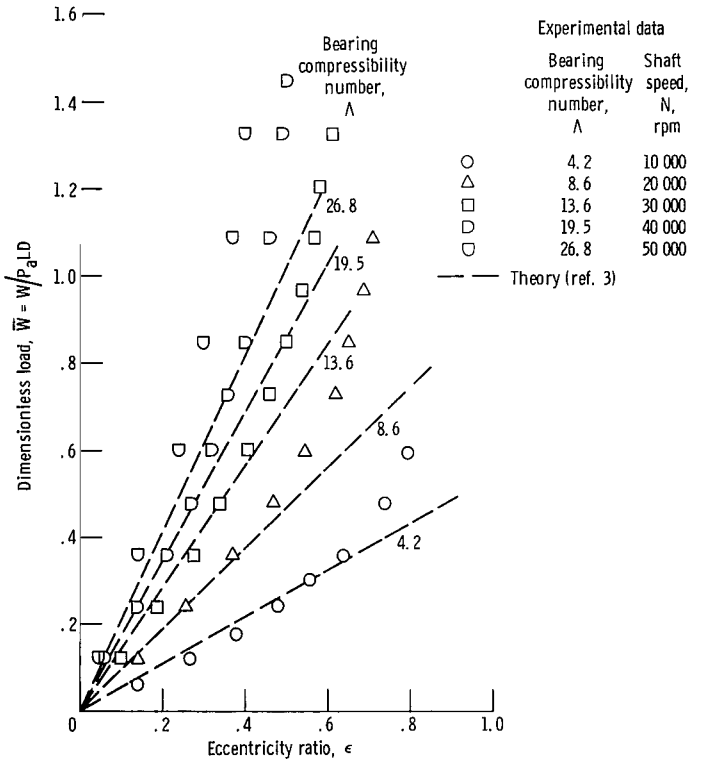

(a) Rotor A-1 (turbine end bearing): helix angle, 30°; number of grooves, 20; ratio of groove width to total width, 0.5; ratio of grooved length to total bearing length, 0.6; ratio of groove clearance to ridge clearance, 2.4; bearing radial clearance, 400 microinches (10.2 μm).

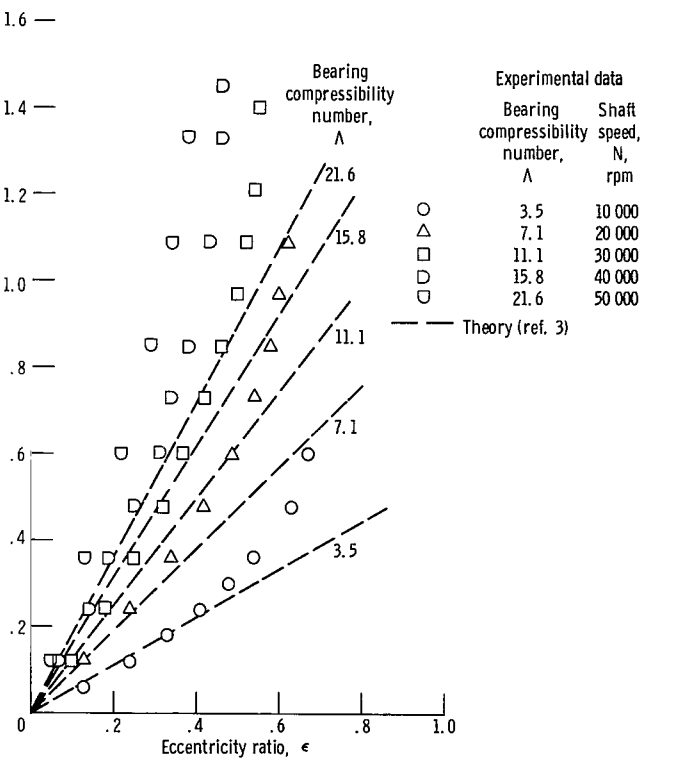

(b) Rotor A-1 (thrust end bearing): helix angle, 30°; number of grooves, 20; ratio of groove width to total width, 0.5; ratio of grooved length to total bearing length, 0.6; ratio of groove clearance to ridge clearance, 2.3; bearing radial clearance, 440 microinches (11.2 μm).

Figure 4. - Dimensionless load as function of eccentricity ratio.

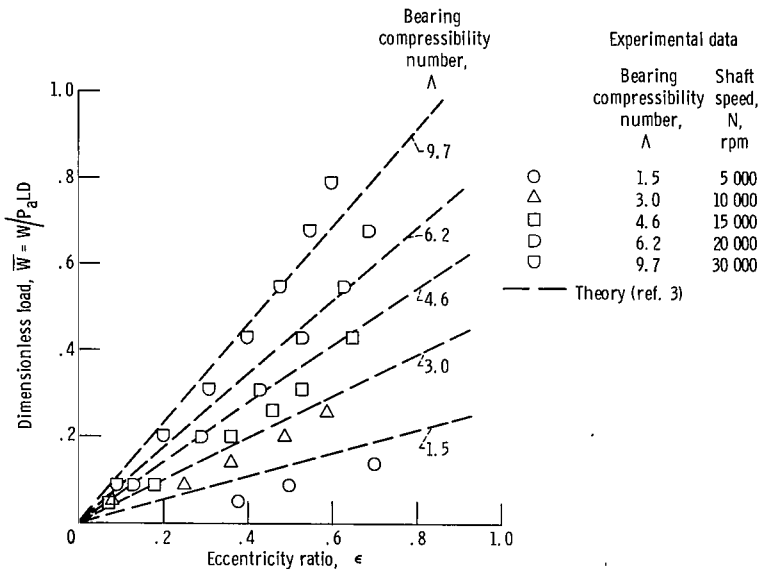

(c) Rotor A-2 (turbine end bearing): helix angle, 35°; number of grooves, 20; ratio of groove width to total width, 0.5; ratio of grooved length to total bearing length, 0.6; ratio of groove clearance to ridge clearance, 2.4; bearing radial clearance, 470 microinches (11.9 μm).

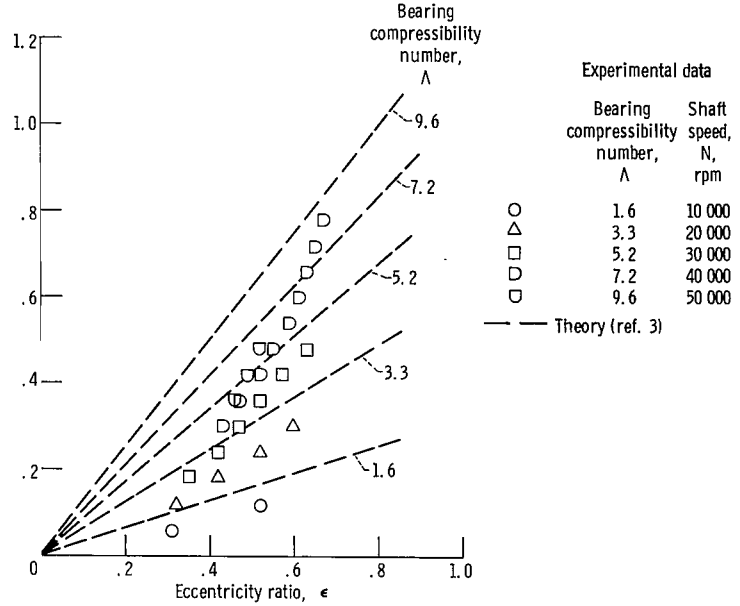

(d) Rotor A-3 (turbine end bearing): helix angle, 35°; number of grooves, 23; ratio of groove width to total width, 0.5; ratio of grooved length to total bearing length, 0.6; ratio of groove clearance to ridge clearance, 1.9; bearing radial clearance, 630 microinches (16 μm).

Figure 4. - Continued.

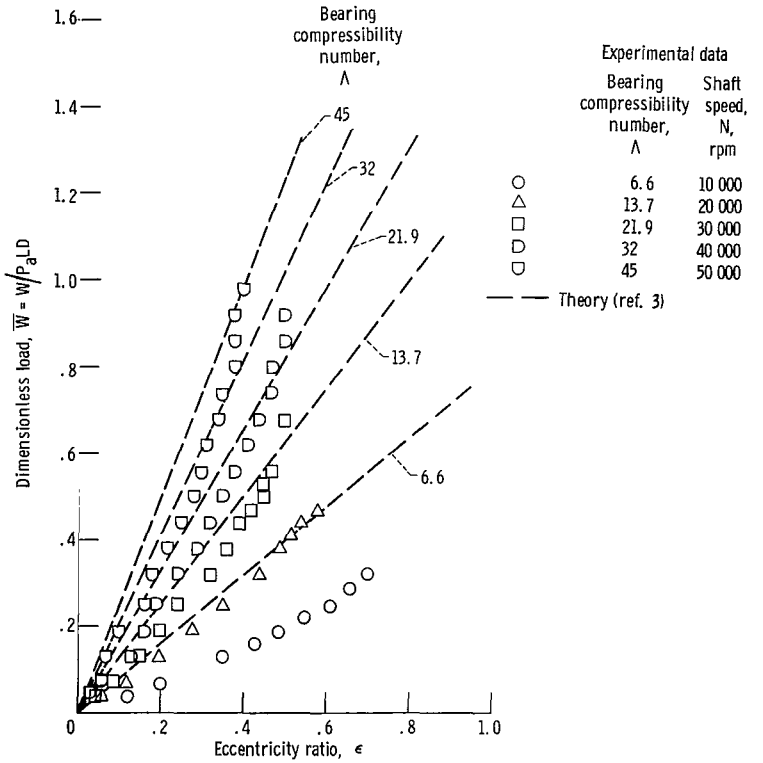

(e) Rotor A-3 (turbine end bearing): helix angle, 35°; number of grooves, 23; ratio of groove width to total width, 0.5; ratio of grooved length to total bearing length, 0.6; ratio of groove clearance to ridge clearance, 2.7; bearing radial clearance, 320 microinches (8.1 μm).

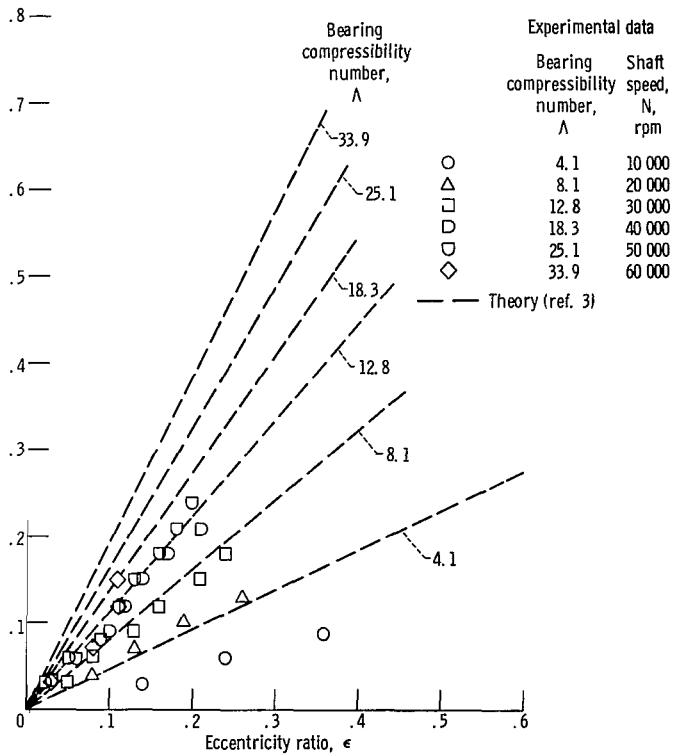

(f) Rotor A-5 (turbine end bearing): helix angle, 40°; number of grooves, 28; ratio of groove width to total width, 0.5; ratio of grooved length to total bearing length, 0.6; ratio of groove clearance to ridge clearance, 2.7; bearing radial clearance, 410 microinches (10.4 μm); bearing length, 1.5 inches (3.81 cm); rotor diameter, 1.5 inches (3.81 cm).

Figure 4. - Continued.

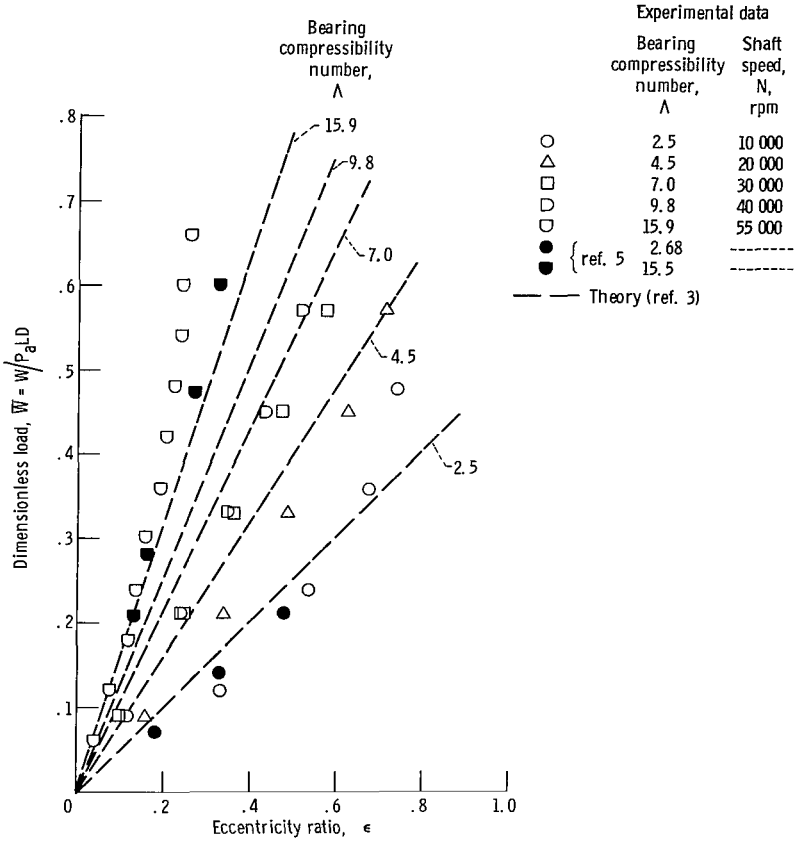

(g) Rotor A-7 (turbine end bearing): helix angle, 40°; number of grooves, 40; ratio of groove width to total width, 0.33; ratio of grooved length to total bearing length, 0.6; ratio of groove clearance to ridge clearance, 2.0; bearing radial clearance, 520 microinches (13.2 μm); bearing length, 1.5 inches (3.81 cm); rotor diameter, 1.5 inches (3.81 cm). Reference 5 rotor: helix angle, 25°; number of grooves, 36; ratio of groove width to total width, 0.35; ratio of grooved length to total bearing length, 0.5; ratio of groove clearance to ridge clearance, 2.33; bearing radial clearance, 495 μin. (12.6 μm).

Figure 4. - Concluded.

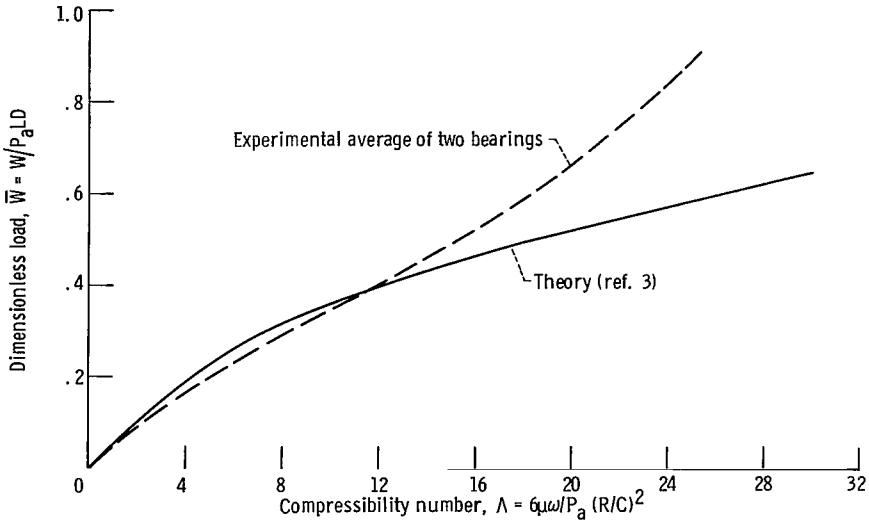

(a) Rotor A-1. Helix angle, 30°; number of grooves, 20; ratio of groove width to total width, 0.5; ratio of grooved length to total bearing length, 0.6; bearing radial clearance: turbine end, 400 microinches (10.2 μm); thrust end, 440 microinches (11.2 μm); ratio of groove clearance to ridge clearance: turbine end, 2.4; thrust end, 2.3.

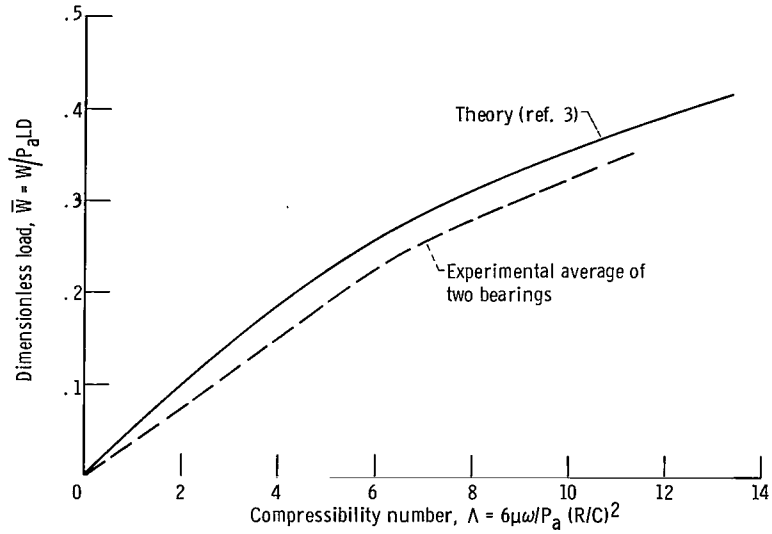

(b) Rotor A-2: helix angle, 35°; number of grooves, 20; ratio of groove width to total width, 0.5; ratio of grooved length to total bearing length, 0.6; bearing radial clearance: turbine end, 470 microinches (11.9 μm); thrust end, 480 microinches (12.2 μm); ratio of groove clearance to ridge clearance: turbine end, 2.4; thrust end, 2.3.

Figure 5. - Comparison of experimental with theoretical load capacity as function of compressibility number. Journal eccentricity ratio, 0.3; bearing length, 1.5 inches (3.81 cm); rotor diameter, 1.5 inches (3.81 cm); atmospheric pressure, 14.4 psia (10 N/cm^2 abs).

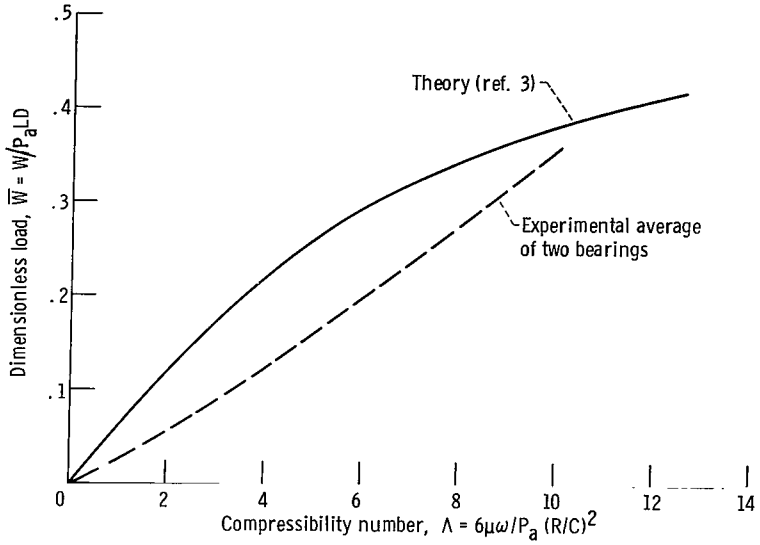

(c) Rotor A-3: helix angle, 35°; number of grooves, 23; ratio of groove width to total width, 0.5; ratio of grooved length to total bearing length, 0.6; bearing radial clearance: turbine end, 630 microinches (16 μm); thrust end, 650 microinches (16.5 μm); ratio of groove clearance to ridge clearance: turbine end, 1.9; thrust end, 1.8.

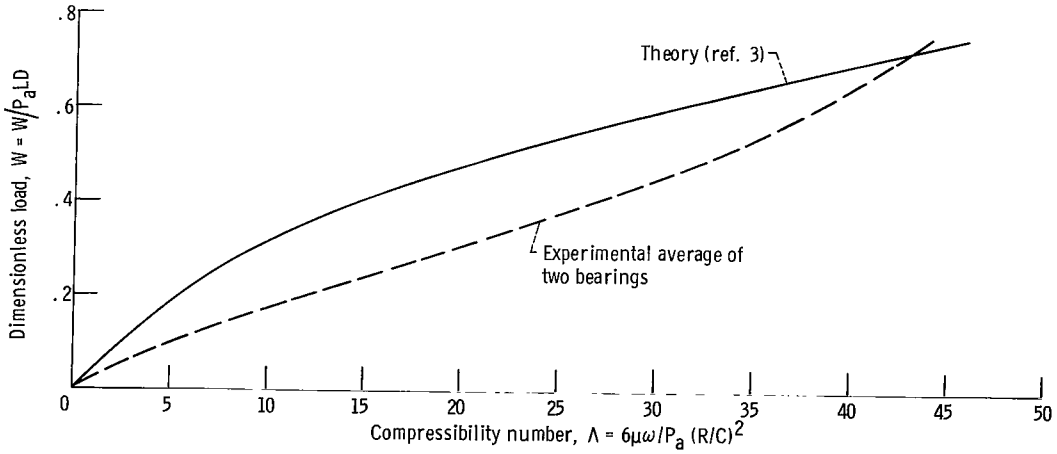

(d) Rotor A-3: helix angle, 35°; number of grooves, 23; ratio of groove width to total width, 0.5; ratio of grooved length to total bearing length, 0.6; bearing radial clearance: turbine end, 320 microinches (8.1 μm); thrust end, 340 microinches (8.6 μm); ratio of groove clearance to ridge clearance: turbine end, 2.7; thrust end, 2.6.

Figure 5. - Continued.

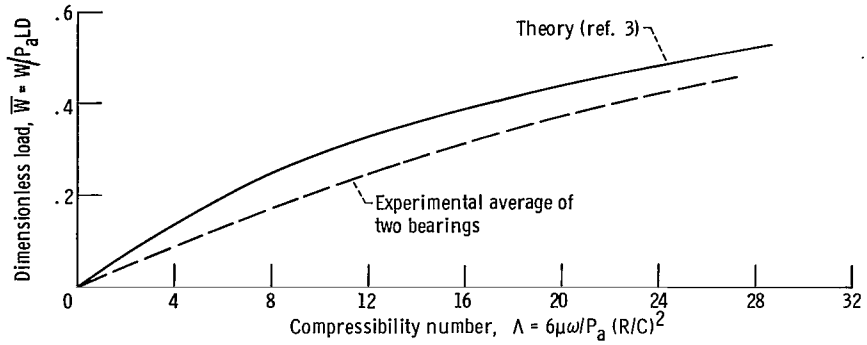

(e) Rotor A-5: helix angle, 40°; number of grooves, 28; ratio of groove width to total width, 0.5; ratio of grooved length to total bearing length, 0.6; bearing radial clearance, 410 microinches (10.4 μm); ratio of groove clearance to ridge clearance: turbine end, 8.7; thrust end, 2.7.

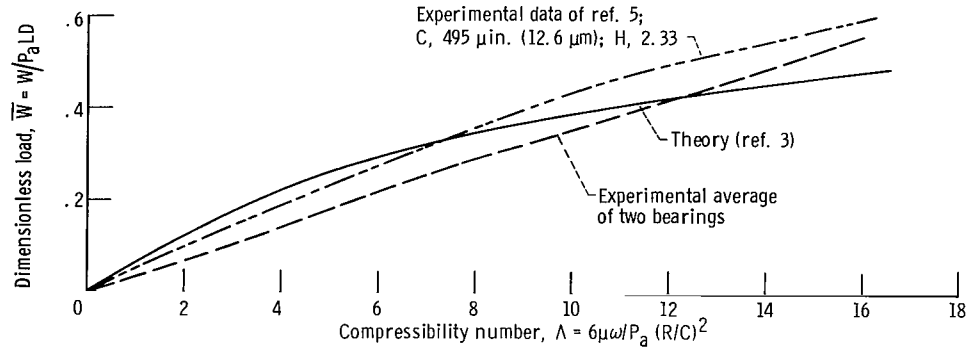

(f) Rotor A-7: helix angle, 40°; number of grooves, 40; ratio of groove width to total width, 0.33; ratio of grooved length to total bearing length, 0.6; bearing radial clearance: turbine end, 520 microinches (13.2 μm); thrust end, 550 microinches (14 μm); ratio of groove clearance to ridge clearance, 2.0.

Figure 5. - Concluded.

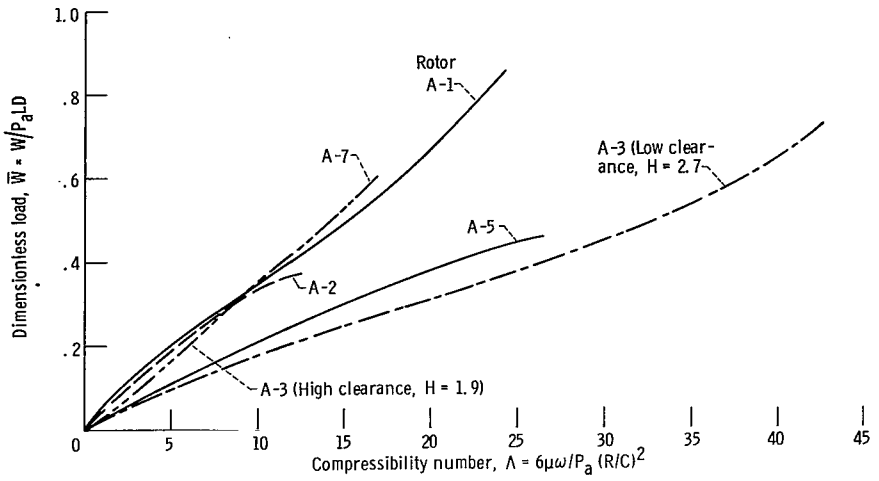

Figure 6. - Comparitive experimental load capacities for five herringbone-grooved rotors at eccentricity ratio of 0.3.

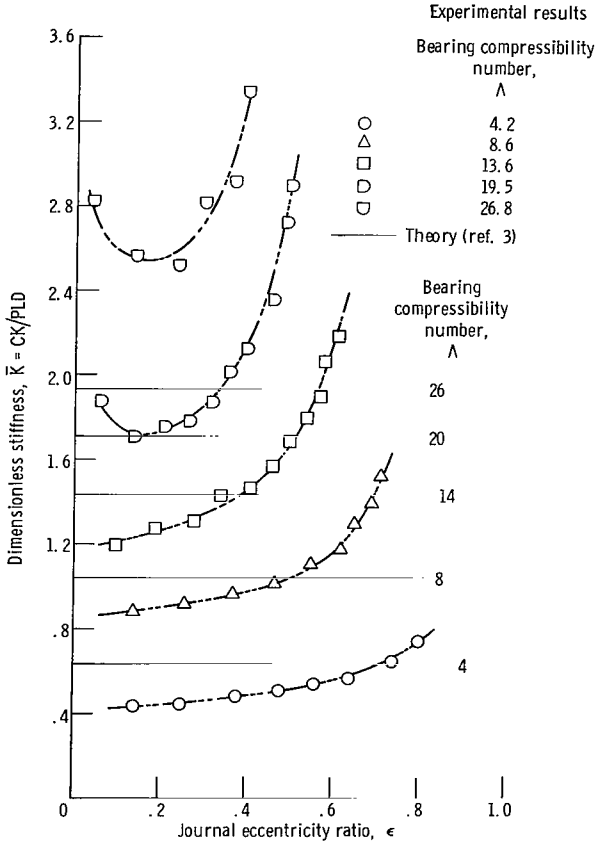

Figure 7. - Comparison of experimental with theoretical dimensionless stiffness as function of eccentricity ratio for rotor A-1. Helix angle, 30°; number of grooves, 20; ratio of groove width to total width, 0.5; ratio of grooved length to total bearing length, 0.6; ratio of groove clearance to ridge clearance, 2.4; bearing radial clearance, 400 microinches (10.2 μm).

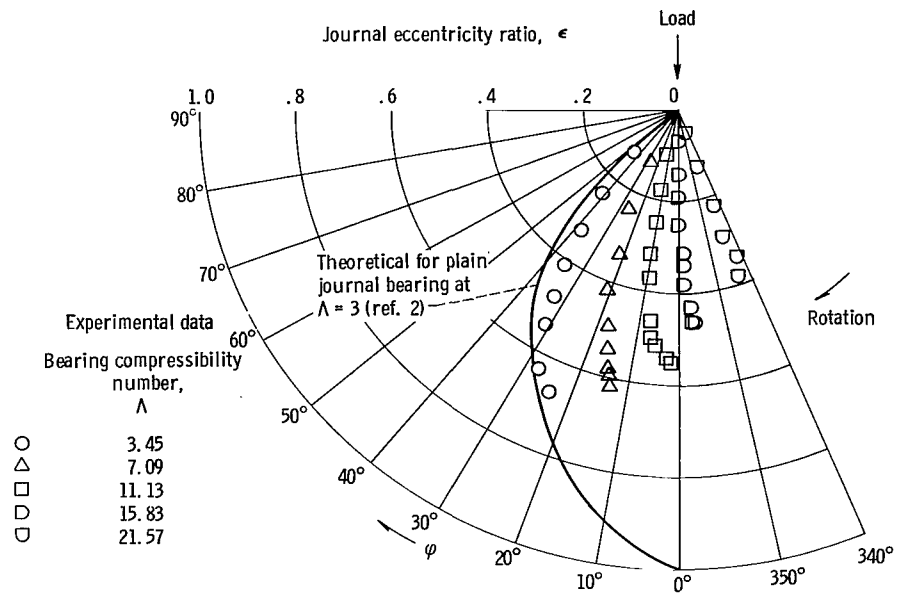

(a) Rotor A-1 (thrust end bearing): helix angle, 30°; number of grooves, 20; ratio of groove width to total width, 0.5; ratio of groove clearance to ridge clearance, 2.3; bearing radial clearance, 440 microinches (11.2 μm).

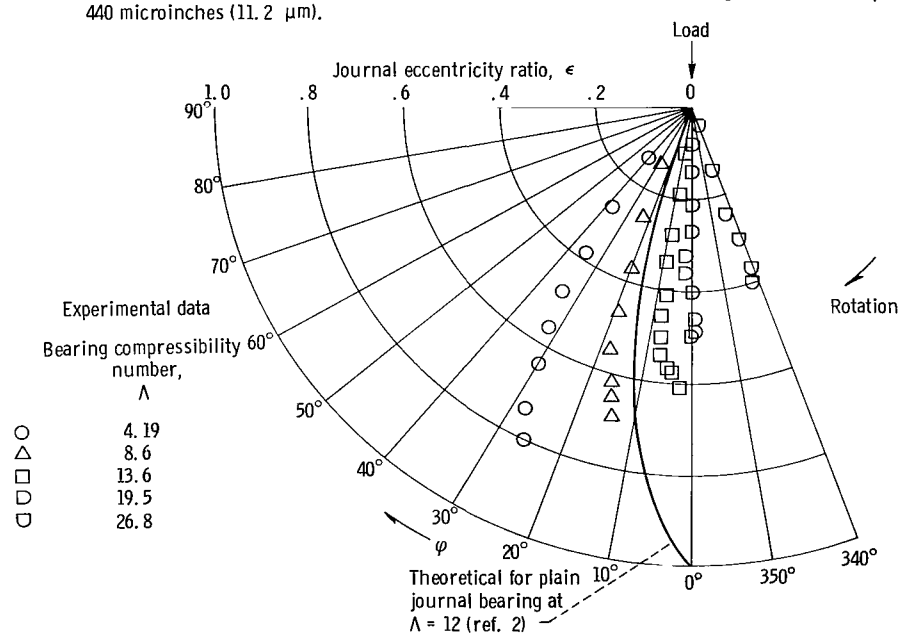

(b) Rotor A-1 (turbine end bearing): helix angle, 30°; number of grooves, 20; ratio of groove width to total width, 0.5; ratio of groove clearance to ridge clearance, 2.4; bearing radial clearance, 400 microinches (10.2 μm).

Figure 8. - Attitude angle as function of eccentricity ratio. Ratio of grooved length to total bearing length, 0.6; length-to-diameter ratio, 1.

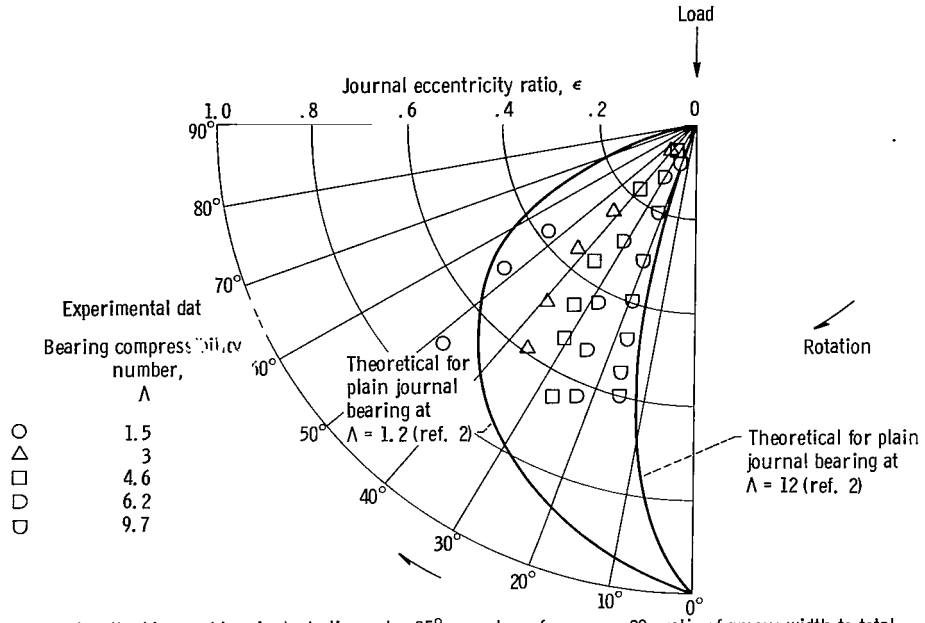

(c) Rotor A-2 (turbine end bearing): helix angle, 35°; number of grooves, 20; ratio of groove width to total width, 0.5; ratio of groove clearance to ridge clearance, 2.4; bearing radial clearance, 470 microinches (11.9 μm).

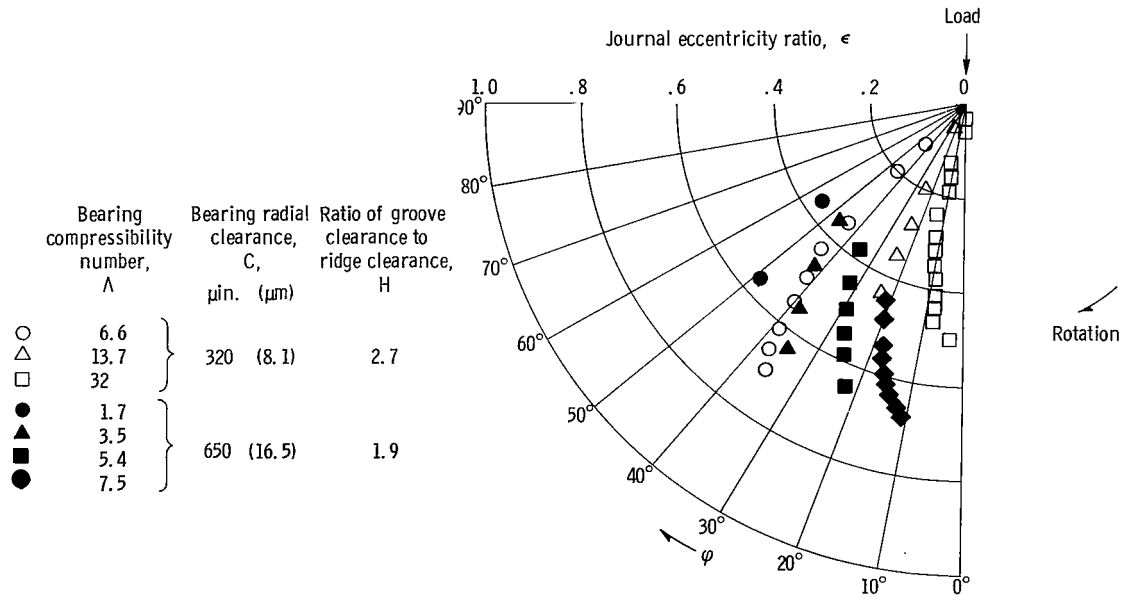

Bearing compressibility number, Λ	Bearing radial clearance, C, μin.	(μm)	Ratio of groove clearance to ridge clearance, H
6.6, 13.7, 32	320	(8.1)	2.7
1.7, 3.5, 5.4, 7.5	650	(16.5)	1.9

(d) Rotor A-3 (turbine end bearing): helix angle, 35°; number of grooves, 23; ratio of groove width to total width, 0.5; ratio of groove clearance to ridge clearance, 2.7; bearing radial clearance, 320 microinches (8.1 μm).

Figure 8. - Continued.

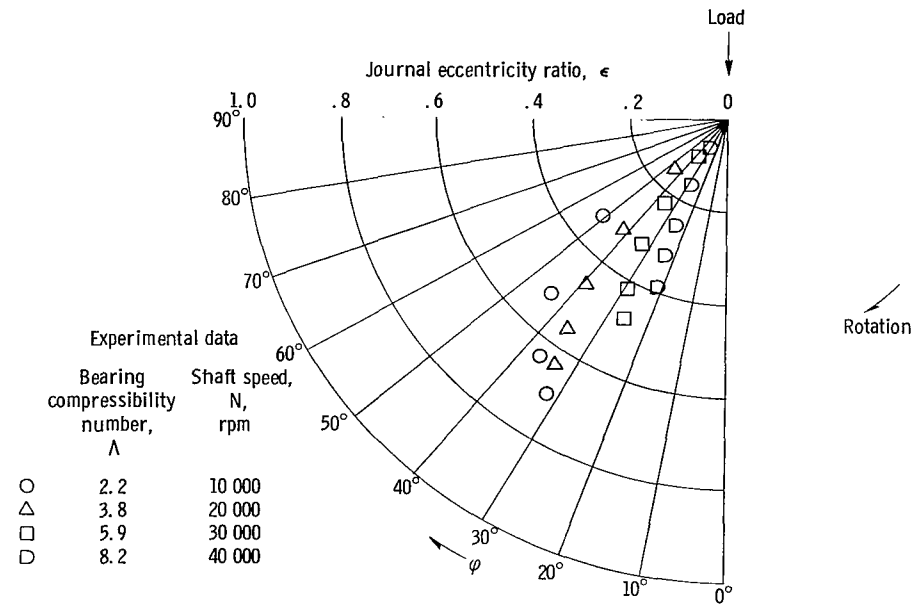

(e) Rotor A-7 (thrust end bearing): helix angle, 40°; number of grooves, 40°; ratio of groove width to total width, 0.33; ratio of groove clearance to ridge clearance, 550 microinches (14 μm).

Figure 8. - Concluded.

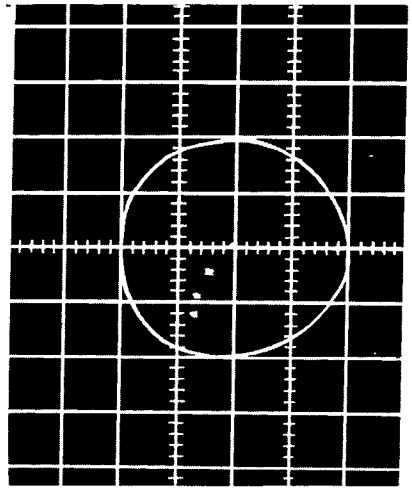

(a) Shaft speed, 10 000 rpm; bearing compressibility number, 2.2.

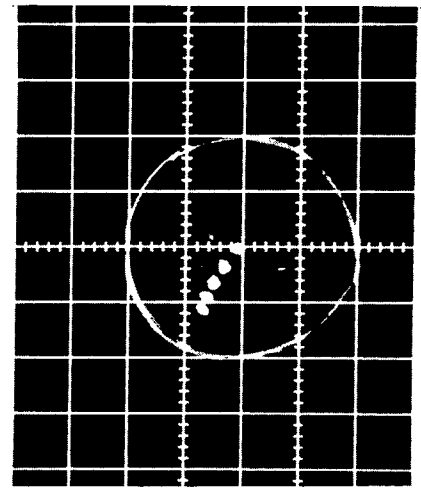

(b) Shaft speed, 20 000 rpm; bearing compressibility number, 3.8.

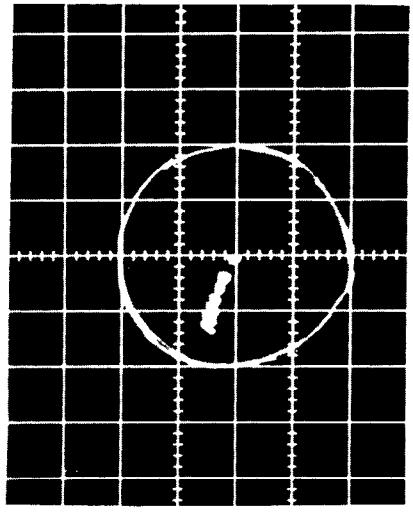

(c) Shaft speed, 30 000 rpm; bearing compressibility number, 5.9.

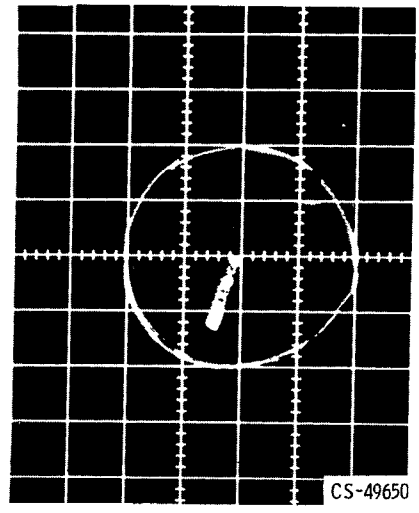

(d) Shaft speed, 40 000 rpm; bearing compressibility number, 8.2.

Figure 9. - Attitude eccentricity locus for rotor A-7 (thrust end bearing). Helix angle, 40°; number of grooves, 40; ratio of groove width to total width, 0.33; ratio of grooved length to total bearing length, 0.6; bearing radial clearance, 550 microinches (14 μm).

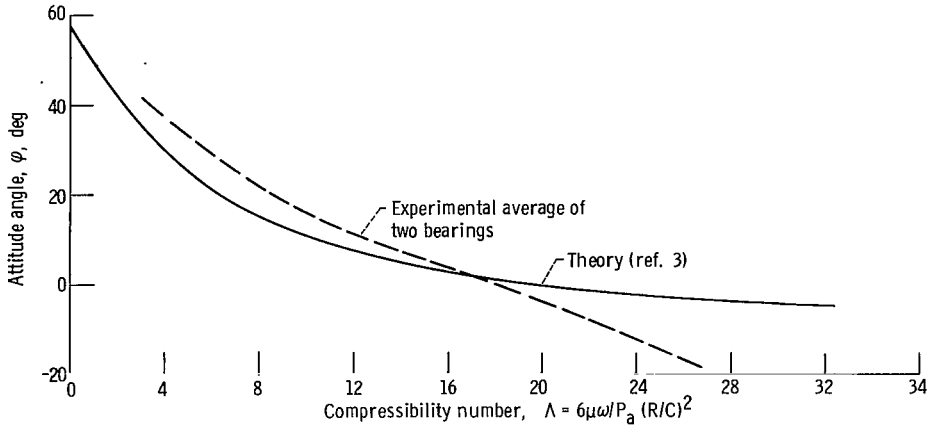

(a) Rotor A-1: helix angle, 30°; number of grooves, 20; ratio of groove width to total width, 0.5; ratio of grooved length to total bearing length, 0.6; bearing radial clearance: turbine end, 400 microinches (10.2 μm); thrust end, 440 microinches (11.2 μm); ratio of groove clearance to ridge clearance: turbine end, 2.4; thrust end, 2.3.

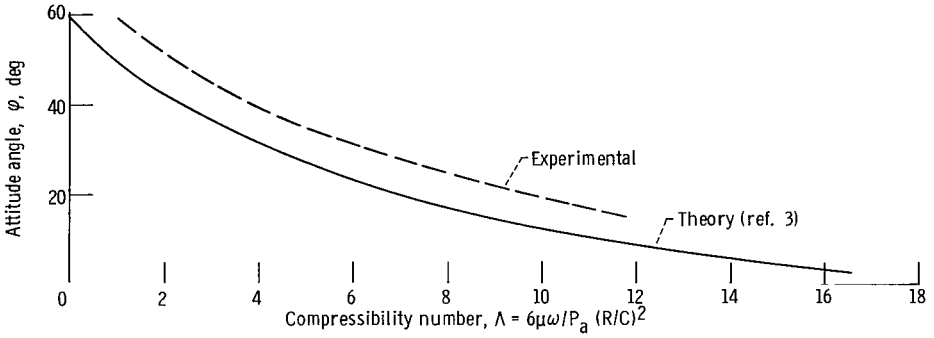

(b) Rotor A-2: helix angle, 35°; number of grooves, 20; ratio of groove width to total width, 0.5; ratio of grooved length to total bearing length 0.6; ratio of groove clearance to ridge clearance, 2.4; bearing radial clearance, 470 microinches (11.9 μm).

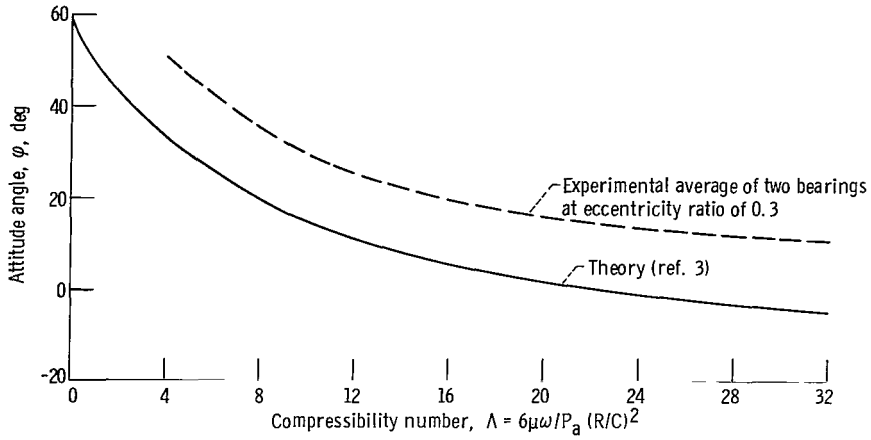

(c) Rotor A-3: helix angle, 35°; number of grooves, 23; ratio of groove width to total width, 0.5; ratio of grooved length to total bearing length, 0.6; bearing radial clearance: turbine end, 320 microinches (8.1 μm); thrust end, 340 microinches (8.6 μm); ratio of groove clearance to ridge clearance: turbine end, 2.7; thrust end, 2.6.

Figure 10. - Comparison of experimental with theoretical attitude angles as function of compressibility numbers at bearing eccentricity ratio of 0.3. Bearing length, 1.5 inches (3.81 cm); rotor diameter, 1.5 inches (3.81 cm).

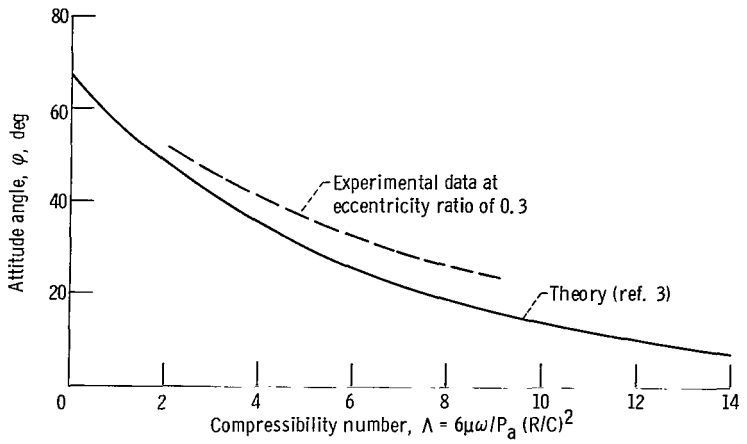

(d) Rotor A-7: helix angle, 40°; number of grooves, 40; ratio of groove width to total width, 0.33; ratio of grooved length to total bearing length, 0.6; ratio of groove clearance to ridge clearance, 2.0; bearing radial clearance, 550 microinches (14 μm).

Figure 10. - Concluded.

NASA-Langley, 1969 —— 15 E-4922

NATIONAL AERONAUTICS AND SPACE ADMINISTRATION
WASHINGTON, D. C. 20546

OFFICIAL BUSINESS

FIRST CLASS MAIL

POSTAGE AND FEES PAID
NATIONAL AERONAUTICS AND
SPACE ADMINISTRATION

"The aeronautical and space activities of the United States shall be conducted so as to contribute . . . to the expansion of human knowledge of phenomena in the atmosphere and space. The Administration shall provide for the widest practicable and appropriate dissemination of information concerning its activities and the results thereof."

—NATIONAL AERONAUTICS AND SPACE ACT OF 1958

NASA SCIENTIFIC AND TECHNICAL PUBLICATIONS

TECHNICAL REPORTS: Scientific and technical information considered important, complete, and a lasting contribution to existing knowledge.

TECHNICAL NOTES: Information less broad in scope but nevertheless of importance as a contribution to existing knowledge.

TECHNICAL MEMORANDUMS: Information receiving limited distribution because of preliminary data, security classification, or other reasons.

CONTRACTOR REPORTS: Scientific and technical information generated under a NASA contract or grant and considered an important contribution to existing knowledge.

TECHNICAL TRANSLATIONS: Information published in a foreign language considered to merit NASA distribution in English.

SPECIAL PUBLICATIONS: Information derived from or of value to NASA activities. Publications include conference proceedings, monographs, data compilations, handbooks, sourcebooks, and special bibliographies.

TECHNOLOGY UTILIZATION PUBLICATIONS: Information on technology used by NASA that may be of particular interest in commercial and other non-aerospace applications. Publications include Tech Briefs, Technology Utilization Reports and Notes, and Technology Surveys.

Details on the availability of these publications may be obtained from:

SCIENTIFIC AND TECHNICAL INFORMATION DIVISION

NATIONAL AERONAUTICS AND SPACE ADMINISTRATION

Washington, D.C. 20546